Desalination and Water Treatment
www.deswater.com

doi: 10.5004/dwt.2021.27083

222 (2021) 246–258
May

Removal of toxic dyes from aqueous solutions by adsorption onto a novel activated carbon prepared from chestnut shell

Mingyang Zhang[a,*], Xinzhe Liu[a], Wenda Li[a], Zhuowei Tan[b], Qian Wang[a], Linhua Zhang[a,*]

[a]*School of Thermal Engineering, Shandong Jianzhu University, Jinan 250101, Shandong, China, Tel./Fax: +86-531-86367629; emails: zhangmingyang18@sdjzu.edu.cn (M.Y. Zhang), liuxinzheoffice@163.com (X.Z. Liu), 1545697454@qq.com (W.D. Li), wangqian18@sdjzu.edu.cn (Q. Wang), zhth0015@sdjzu.edu.cn (L.H. Zhang)*
[b]*College of New Energy, China University of Petroleum (East China), 266580 Shandong, China, Tel./Fax: +86-532-86981865; email: tanzhuowei1990@126.com*

Received 28 July 2020; Accepted 23 January 2021

ABSTRACT

Chestnut shell offers an abundant, renewable and low-cost precursor for the preparation of activated carbon. In this study, a novel activated carbon was prepared from the chestnut shell (CnSAC) by chemical activation with $ZnCl_2$. Based on the N_2 adsorption/desorption isotherm, it is concluded that more micro-pores are developed on the precursor with pore size falls in the range of 0–3 nm. And the X-ray diffraction analysis shows that amorphous carbon and graphite carbon coexist in CnSACs. Moreover, the CnSACs were used to remove methylene blue (MB) from an aqueous solution. Batch adsorption experiments were performed as a function of impregnation mass ratio, impregnation time, activation temperature, activation time and dye solution pH. Besides, the Langmuir, Freundlich and Dubinin–Radushkevich models were applied to describe the equilibrium isotherms. The results showed that equilibrium data fitted well for the Langmuir adsorption isotherms with correlation coefficients of 0.99. The adsorption kinetics of MB were discussed by pseudo-first-order, pseudo-second-order, Elovich and intraparticle diffusion models, which showed that the adsorption followed pseudo-second-order reaction with regard to the intraparticle diffusion rate. Moreover, the maximum adsorption of MB onto CnSACs is 1,489.88 mg/g (impregnation mass ratio: 12.5, impregnation time: 27 h, activation temperature: 600°C, activation time: 75 min, initial MB dye concentration: 600 mg/L). Compared with the ACs prepared from different raw materials, the chestnut shell can be used as a raw material for the preparation of high adsorption performance ACs for the treatment of colored wastewater.

Keywords: Dyes; Chestnut shell; Removal; Activated carbon; Adsorption

1. Introduction

Dyes are widely used in textile, food, leather, cosmetics, paper, lithography, plastics industries [1,2]. It is estimated that more than 100,000 different kinds of commercial dyes with over 700,000 tons are produced annually. And about 10%–20% of dyes are discharged in water resources as waste effluents in their production and application [3]. The dyes diffusing into the water bodies lead to colored wastewater, which is rich in color, pH, chemical oxygen demand, biological oxygen demand and turbidity. Besides, the dyes molecules in colored wastewater obstruct sunlight from reaching the water system, which slows down

* Corresponding authors.

photosynthesis and causes the decline of dissolved oxygen in colored wastewater [4,5]. More seriously, most of the dyes are toxic and carcinogenic. Therefore, from the living being's health perspective, the treatment of the colored wastewater is becoming an issue that needs taking care of desperately.

Due to the high organic matter and poor biodegradability of colored wastewater, great efforts have been invested in color removal and organic matter degradation. The most commonly used methods of color removal from industrial effluents include coagulation, air flotation, adsorption, membrane separation, ion exchange, oxidation, photochemistry and biological treatment [6–13]. Among the methods stated above, adsorption has been identified to be superior compared with other methods in terms of cost-effectiveness, simplicity of design, easy operation and environmental benignity. The adsorption can be achieved by using adsorbents with a high adsorptive capacity and selectivity. Thus, the characteristics of adsorbents are the key factors to affect the adsorption capacity. Various adsorbents have been utilized for color removal such as activated carbon, kaolin, synthetic polymer, clay, slag [14–17]. However, activated carbon appears to be the first option in the treatment of colored wastewater.

Activated carbon is a porous material with a high surface area, which can be produced based on coal [18], petroleum coke [19] and biomass [20]. Compared with the coal and petroleum coke-based activated carbons, biomass-based activated carbons are the most promising porous materials for the following reasons. Firstly, the raw materials are abundant and cost-effective. Secondly, they have no adhesiveness and need not vis-breaking treatment. Lastly, the preparation process is simple and easy to operate [21]. Therefore, plenty of agricultural by-products and waste materials are used for the production of activated carbons including rattan sawdust [22], jute fiber [23], fruit stones and nutshells [24], rice hull [25], cola nutshell [26], dead leaves [27], dross licorice [28], eucalyptus residue [29], bamboo chip [30], orange peel [31], mushroom [32], liquefied wood [33], etc.

Chestnut is a Fagaceae plant, which is widely distributed and rich in germplasm resources [34]. Besides, chestnut is an excellent source of unsaturated fatty acids, minerals and vitamin C. However, the chestnut shell is usually discarded as a residue during post-harvesting processing, which causes a great waste of resources. Thus, some studies have been focused on the resource utilization of chestnut shells [35,36].

In this work, a novel porous activated carbon was prepared from the chestnut shell (CnSAC) by chemical activation ($ZnCl_2$) in the absence of air. The chestnut shells were obtained from wild forests. Then the CnSACs were used as the adsorbents to remove methylene blue (MB) from the aqueous solution. The effect of impregnation mass ratio, impregnation time, activation temperature, activation time and pH on the adsorption capacity of MB were investigated. Moreover, the adsorption equilibrium and kinetic studies were also carried out to understand the adsorption process. The aims of this work are to provide a novel porous activated carbon for colored wastewater treatment and a promising treatment method of agricultural residues.

2. Experimental methods

2.1. Materials

The MB (chemical formula: $C_{16}H_{18}ClN_3S{\cdot}3H_2O$; formula mass: 373.90 g/mol) was supplied by Tianjin Zhiyuan Chemical Reagent Co., Ltd., (China) with the purity greater than 98.5%. And its chemical structure is shown in Fig. 1. Besides, potassium hydroxide and HCl were purchased by Jinan Xiaoshi Chemical Co., Ltd., China. A stock solution of MB (1,000 mg/L) was prepared and suitably diluted to the required concentration with deionized water. And the concentrations of the MB dye were determined at 665 nm, using a UV spectrophotometer (Pgeneral Model: T6, China). Besides, the ultimate analysis of the chestnut shell was conducted using an elements analyzer (Vario ELIII, Elementar) and the result is presented in Table 1. Remarkably, all the chemicals were of analytical reagent grade.

2.2. Preparation of CnSACs

Firstly, the chestnut shells were left to dry at 80°C for 2 h, then they were cut into small pieces and sieved to average particle size (75 μm). Secondly, the chestnut shell powder was impregnated in $ZnCl_2$ aqueous solution (mass fraction of $ZnCl_2$: 25%) for 24 h. After impregnation, the mixture was carbonized in a tube furnace at 600°C under a nitrogen atmosphere for 90 min with a heating rate of 10°C/min and a N_2 flow of 2.0 L/min. Lastly, the obtained chestnut shell-based activated carbons (CnSACs) were washed with deionized water and dried at 102°C for 24 h. Remarkably, the chestnut shell powder was impregnated in $ZnCl_2$ aqueous solution with different impregnation mass ratios (mass ratio of $ZnCl_2$ aqueous solution to chestnut shell powder, r_i) of 5, 7.5, 10, 12.5, 15, 20 and 25, respectively. And the impregnation time (t_i) varied at 6, 12, 18, 21, 24, 27, 30 and 36 h. Besides, the CnSACs were prepared at different activation temperatures (T_a), that is, 400°C, 450°C, 500°C, 550°C, 600°C, 650°C and 700°C. And the activation time (t_a) was adjusted to seven levels, which were 30, 45, 60, 75, 90, 120 and 150 min.

2.3. Characterization

The surface morphology and fundamental physical properties of CnSACs were analyzed by scanning electron microscope (SEM, Hitachi S-4800, 7593-H, Japan). And the porous characterization of CnSACs was investigated by the multi-point adsorption of nitrogen at 77 K using Autosorb iQ, supplied by Quantachrome Corporation, USA.

Table 1
Ultimate analysis of chestnut shell

Elements	wt.%
C	52.66
H	5.13
O	40.84
N	0.58
S	0.01

Fig. 1. Chemical structure of MB.

The total surface area was calculated from the Brunauer–Emmett–Teller (BET) method and pore size distributions were calculated using Barrett–Joyner–Halenda method based on the nitrogen adsorption and desorption data. Moreover, the X-ray diffraction (XRD) spectra analysis was done on an X-Ray Diffractometer (Ultima IV, Japan).

2.4. Adsorption experiments

Several factors affecting the adsorption capacity of MB, that is, impregnation mass ratio, impregnation time, activation temperature and activation time were studied. For each experimental run, 8.0 mg of CnSAC was stirred with 80 mL of MB solution with the same concentration (300 mg/L) in a 150 mL stoppered conical flask. And then the flasks were put in a temperature-controlled shaking water bath at a constant speed of 180 rpm for 24 h.

Besides, the adsorption equilibrium and adsorption kinetic studies were conducted. Adsorption equilibrium experiment was performed in a set of stoppered conical flasks, 8.0 mg of CnSAC stirred with 80 mL solutions of MB dye at different initial concentrations (100, 200, 300, 400, 500, 600, 700 mg/L) were placed in these flasks. Then the flasks were put in a temperature-controlled shaking water bath at 180 rpm for 24 h at different temperatures of 30°C, 40°C and 50°C, respectively. In the adsorption kinetic studies, 8.0 mg of CnSAC was dosed in a series of MB solutions with a same concentration (300 mg/L). The residual concentrations of each flask was measured at pre-set time intervals (2, 5, 7, 10, 15, 20, 30, 40, 50, 60, 70, 80, 90 min), respectively.

The equilibrium adsorption capacity was calculated from the equation [37]:

$$q_e = \frac{\left(C_0 - C_e\right)V}{w} \tag{1}$$

where q_e (mg/g) is the equilibrium adsorption capacity of MB, C_e is the MB concentration at equilibrium, V(L) is the volume of MB solution and w(g) is the weight of CnSACs.

3. Results and discussion

3.1. Characterization of CnSACs

The preparation parameters and BET surface areas of three typical CnSACs (CnSAC-01, CnSAC-02, CnSAC-03), are given in Table 2. In addition, the SEM images of the three typical CnSACs are shown in Fig. 2. The images show that the pore structures of CnSAC-01 is more developed than that of CnSAC-02 and CnSAC-03, which can be explained by the abundant abnormity protrusions, depressions and folds on the surface of CnSAC-01 as shown in Figs. 2a and b. Thereby, the surface characteristics of CnSAC-01 result in high surface area and more adsorption sites for the adsorbate. On the contrary, there exist some areas where pore structures are not formed as shown in Figs. 2c–f. The difference in surface morphology is consistent with the difference of BET surface areas in Table 2. Thus, it can be seen that the preparation parameters have a significant influence on the surface morphology of CnSACs.

Table 2
Three typical CnSACs

Samples	r_i	t_i (h)	T_a (°C)	t_a (min)	BET surface area (m^2/g)
CnSAC-01	12.5	27	600	75	1,539.410
CnSAC-02	10	24	600	75	1,524.647
CnSAC-03	10	27	600	90	954.445

Fig. 3 shows the pore size distribution curve and accumulative pore volume vs pore width of CnSAC-01. The results show that the pore size of CnSAC-01 falls in the range of 0–3 nm. This indicates that more micro-pores are developed on the precursor under the activation of $ZnCl_2$, which greatly enriches the diversity of pore structure. Moreover, the XRD analysis was performed to investigate the crystallinity of CnSAC-01, as shown in Fig. 4. It is clear that there are two obvious peaks that represent to amorphous carbon at a 2θ value of 22.42° and 42.56°. This phenomenon indicates that amorphous carbon (amorphous state) and graphite carbon coexist in carbon materials [38].

3.2. Investigations of preparation and sorption parameters

3.2.1. Effect of impregnation mass ratio

The effect of impregnation mass ratio on the adsorption capacity of MB (q_e) onto CnSACs was studied as shown in Fig. 5. It can be seen that the adsorption capacity of MB was found to increase firstly and then decrease with the increase of impregnation mass ratio. The adsorption capacity reached the peak value (994.18 mg/g) when the impregnation ratio was 12.5. The results indicated that there existed an optimal impregnation mass ratio for the pore structure formation of CnSACs. With the increase of impregnation mass ratio, the pore structure of CnSACs was getting more developed under the influence of polycondensation and dehydration caused by $ZnCl_2$. But as the concentration of $ZnCl_2$ was further increased, the formed micropores were etched into mesopores or even macropores. Thus the developed pore structure of CnSACs collapsed, and the adsorption capacity of MB decreased consequently.

3.2.2. Effect of impregnation time

The effect of impregnation time on the adsorption capacity of MB (q_e) onto CnSACs was studied as shown in Fig. 6. The results show that the adsorption capacity of MB first increases, and attains maximum value when the impregnation time is 27 h, then decreases when the impregnation time was beyond 27 h. In addition, the maximum adsorption

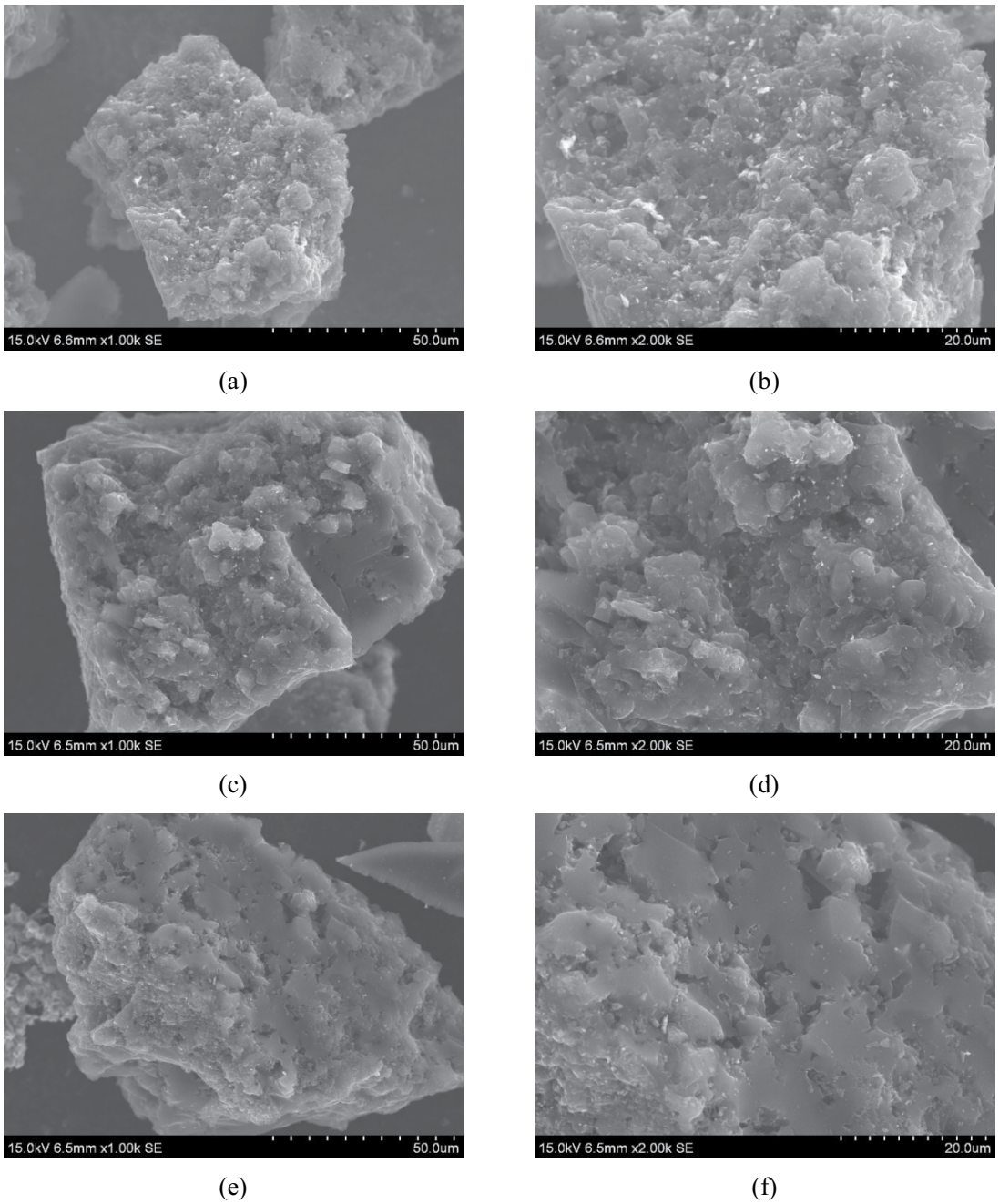

Fig. 2. Scanning electron micrograph of CnSACs: (a and b) CnSAC-01, (c and d) CnSAC-02, (e and f) CnSAC-03.

capacity of MB is 1,013.51 mg/g. This may be due to that the developed pore structure gradually formed by the erosion of $ZnCl_2$ with time. However, when the impregnation time was more than 27 h, the micropores and mesopores formed were destroyed into macropores or even collapse. Therefore, the increase of pore size led to the decrease of the adsorption capacity of MB.

3.2.3. Effect of activation temperature

The effect of activation temperature on the adsorption capacity of MB (q_e) onto CnSACs is shown in Fig. 7. Similarly, the changing trend is to increase firstly and then decrease. The adsorption capacity of MB reached the peak value (1,013.51 mg/g) when the activation temperature was 600°C. The increase of activation temperature was conducive to the pore structure formation under the activation of $ZnCl_2$ at a lower temperature range. Therefore, the number of micropores gradually increased with the increase of activation temperature. But the wall of the formed micropores was ablated and collapsed to form larger pores when the activation temperature was over 600°C. This led to the decrease of the specific surface area of CnSACs and further affected the adsorption capacity of MB.

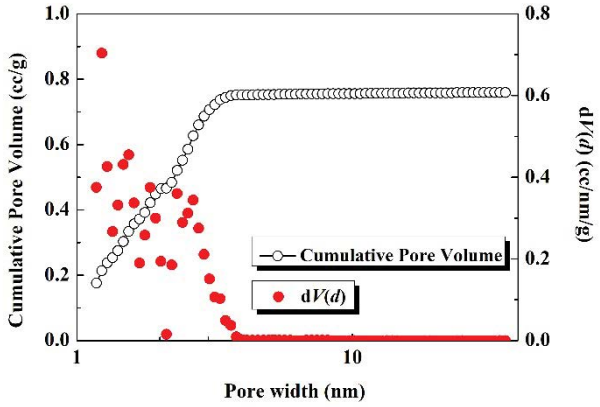

Fig. 3. Pore size distribution and accumulative pore volume curve of CnSAC-01.

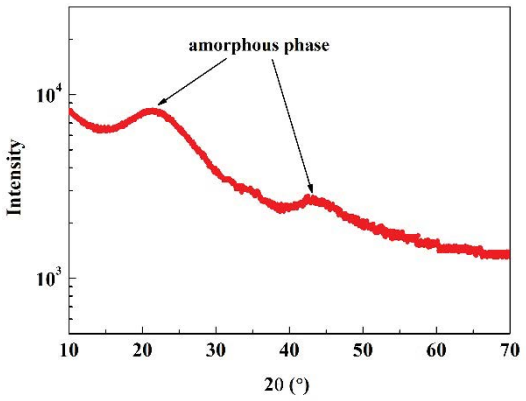

Fig. 4. X-ray diffraction plots of CnSAC-01.

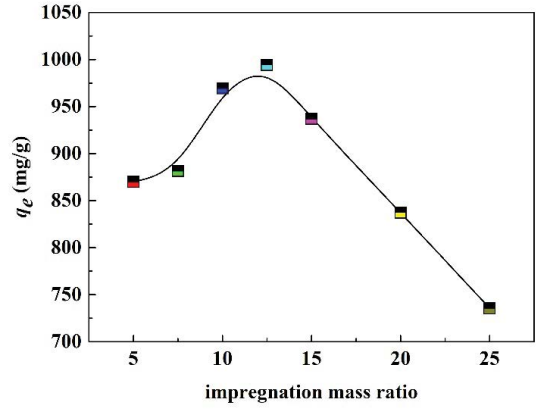

Fig. 5. Effect of impregnation mass ratio on the adsorption capacity of MB at t_i = 24 h; T_a = 600°C; t_a = 90 min; pH = 7.5.

3.2.4. Effect of activation time

Fig. 8 shows the effect of activation time on the adsorption capacity of MB (q_e) onto CnSACs. As shown in Fig. 8, the adsorption capacity of MB increased with the

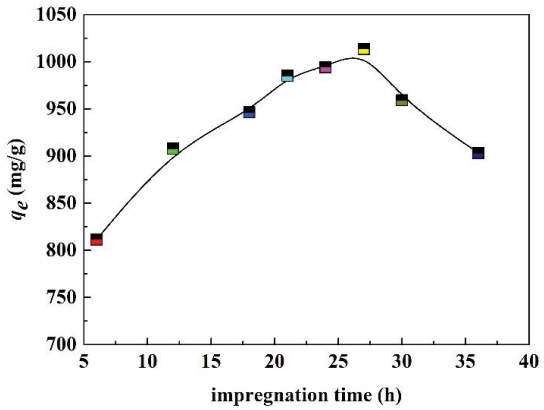

Fig. 6. Effect of impregnation time on the adsorption capacity of MB at r_i = 12.5; T_a = 600°C; t_a = 90 min; pH = 7.5.

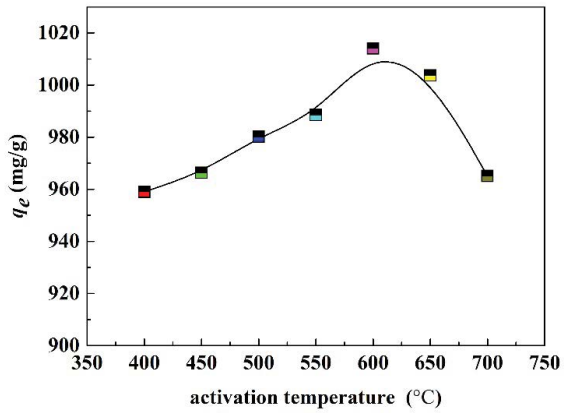

Fig. 7. Effect of activation temperature on the adsorption capacity of MB at r_i = 12.5; t_i = 27 h; t_a = 90 min; pH = 7.5.

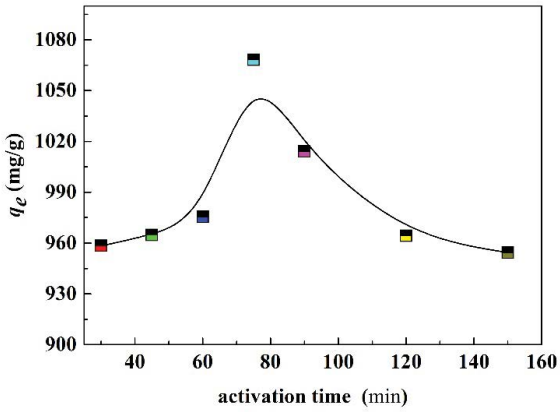

Fig. 8. Effect of activation time on the adsorption capacity of MB at r_i = 12.5; t_i = 27 h; T_a = 600°C; pH = 7.5.

increase of activation time, when the activation time was shorter than 75 min. However, the adsorption capacity of MB decreased when the activation time was longer than 75 min. This may be due to that impurity in the chestnut

shell gradually reduces at the beginning of carbonization and activation. With the evaporation of water vapor, pores were gradually formed on the carbon surface, and the specific surface area also increased. As a result, the adsorption capacity of MB increased. However, when the activation time was longer than 75 min, carbon was burned out gradually and the carbon skeleton began to collapse. Consequently, some micropores formed were destroyed and expanded to mesopores or macropores. Thus the adsorption capacity of MB decreased.

3.2.5. Effect of dye solution pH

Fig. 9 illustrates the effect of dye solution pH on the adsorption capacity of MB (q_e) onto CnSACs. The results indicate that the adsorption capacity of MB is clearly pH-dependent, which presents the trend that first increases and then decreases with the increase of dye solution pH. And the maximum adsorption capacity of MB was observed at dye solution pH: 5.0. The dye solution pH may affect the ionization degree and structure of adsorbate, surface charge, functional group and active site of the adsorbent. Under acidic conditions (i.e., dye solution pH 2.5–5.0), the increase of MB adsorption capacity might be due to the proton reduction in an aqueous medium. However, the decrease of MB adsorption capacity with a further increase in dye solution pH from 5.0 to 11.5 was caused by surface protonation [39]. Therefore, the dye solution pH should be was optimized at 5.0 for the best adsorption.

3.3. Adsorption equilibrium analysis

The adsorption isotherms of CnSACs towards MB are shown in Fig. 10. It could be seen that the adsorption capacities of MB increased with the increase of the initial concentration of MB (C_e). Higher initial concentration may lead to a stronger driving force to promote diffusion of MB molecules from aqueous solution to CnSACs. Besides, the maximum adsorption amount of MB increased with the increase of temperature, which are 1,119.13; 1,216.64 and 1,429.88 mg/g, respectively. With the increase of temperature, the viscosity of MB solution decreased, and the molecular motion and collision were intensified, which promoted the diffusion of adsorbate molecules and accelerated the adsorption process.

Moreover, the adsorption isotherm can be approximately expressed by an appropriate function based on the isothermal adsorption model, which can reveal the relationship between the equilibrium concentration of MB and the adsorption capacity of CnSACs. In this work, the isotherms experimental data were fitted by three models (Langmuir model, Freundlich model, and Dubinin–Radushkevich model), respectively. The fitting results are shown in the following sections.

3.3.1. Langmuir model

Langmuir's theory is one of the frequently-used adsorption isotherm equations, which assumes that there are a certain number of adsorption sites on the surface of the adsorbent, and each adsorption site can only adsorb one molecule or atom [40]. The Langmuir theory can be expressed by [41]:

$$\frac{C_e}{q_e} = \frac{1}{q_m K_L} + \frac{C_e}{q_m} \tag{2}$$

where C_e is the equilibrium concentration (mg/L), q_e is the capacity of MB adsorbed at equilibrium (mg/g), q_m (mg/g) and K_L (L/mg) are Langmuir constants.

In order to analyze the Langmuir model thoroughly, dimensionless separation factor (R_L) was calculated according to experimental data, which can be calculated by the Eq. (3) [42]:

$$R_L = \frac{1}{1 + K_L C_0} \tag{3}$$

where C_0 is the initial methylene blue dye concentration, mg/L.

The fitting results of the Langmuir model are shown in Table 3 and Fig. 11. As shown in the results, the fitting of experimental data is good and the correlation coefficients,

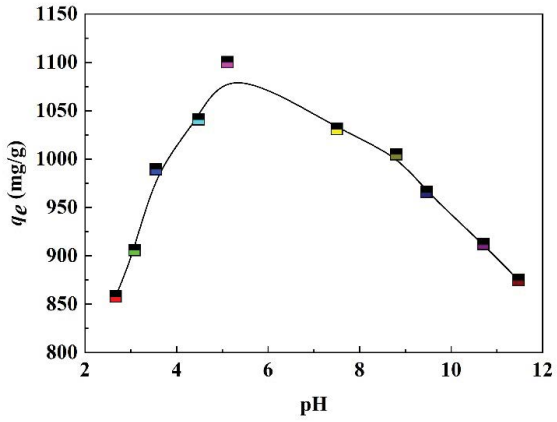

Fig. 9. Effect of dye solution pH on the adsorption capacity of MB at r_i = 12.5; t_i = 27 h; T_a = 600°C; t_a = 75 min.

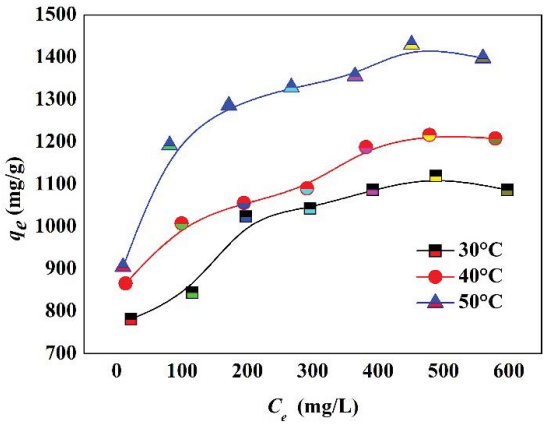

Fig. 10. MB dye adsorption isotherm onto CnSACs.

Table 3
Langmuir isotherm constants for the adsorption of MB

Adsorption temperature (°C)	30	40	50
q_m (mg/g)	1,143.219	1,248.327	1,435.870
K_L (L/mg)	0.0426	0.0442	0.0683
R_L	0.0324~0.190	0.0313~0.185	0.0205~0.128
R^2	0.997	0.996	0.998

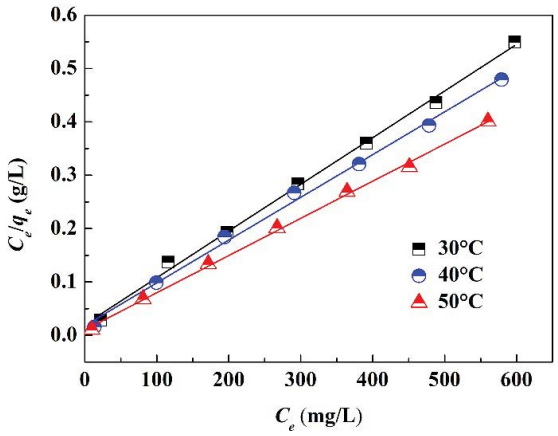

Fig. 11. Langmuir isotherms for adsorption of MB onto CnSACs.

R^2, is higher than 0.99. Besides, the saturated adsorption capacity of MB increased with the increase of temperature, which are 1,143.219; 1,248.327 and 1,435.870 mg/g at 30°C, 40°C and 50°C, respectively. K_L increased from 0.0426 to 0.0683 L/mg. Therefore, the results showed that the endothermic reaction occurred in the adsorption of MB onto CnSACs. Moreover, the dimensionless separation factor (R_L) is in the range of 0–1, thus the adsorption is easy to occur.

3.3.2. Freundlich model

The Freundlich isotherm model is an empirical model, which is related to the adsorption capacity and adsorption heat based on the adsorption theory on the heterogeneous surface [43]. The amount of solute adsorbed (q_e) is related to the equilibrium concentration of solute in solution (C_e) as shown in Eq. (4) [44]:

$$q_e = K_F C_e^{\frac{1}{n}} \tag{4}$$

Therefore, Eq. (4) can be expressed linearly by Eq. (5):

$$\ln q_e = \ln K_F + \frac{1}{n}\ln C_e \tag{5}$$

where K_F is the Freundlich model constant, which is related to the binding energy.

As shown in Table 4 and Fig. 12, the correlation coefficient (R^2) of the Freundlich isotherm model fell into 0.895~0.983. Compared with the Langmuir model, the correlation is lower relatively.

3.3.3. Dubinin–Radushkevich model

Dubinin–Radushkevich's model is based on the adsorption potential theory. The adsorption potential theory can be used to judge the mechanism of the adsorption process, which is more applicable than the Langmuir isotherm model. The Dubinin–Radushkevich isotherm model is expressed by Eq. (6) [27]:

$$\ln q_e = \ln q_m - B\left[RT\ln\left(1+\frac{1}{C_e}\right)\right]^2 \tag{6}$$

where B is a constant related to the sorption energy (mol²/J²), R is the ideal gas constant (8.314 J/mol K), T is the Kelvin temperature.

The fitting results are shown in Table 5 and Fig. 13. The energy-related to adsorption in Table 6 can be obtained by Eq. (7) [45]:

$$E = \frac{B^{-1/2}}{\sqrt{2}} \tag{7}$$

As shown in Table 5 and Fig. 13, the energy values range between 1 and 8 kJ/mol, which indicates that the adsorption is due to physical interactions between adsorbent and

Table 4
Freundlich isotherm constants for the adsorption of MB

Adsorption temperature (°C)	30	40	50
K_F [(mg/g)(L/mg)$^{1/n}$]	531.658	670.484	717.663
$1/n$	0.116	0.0917	0.110
R^2	0.895	0.954	0.983

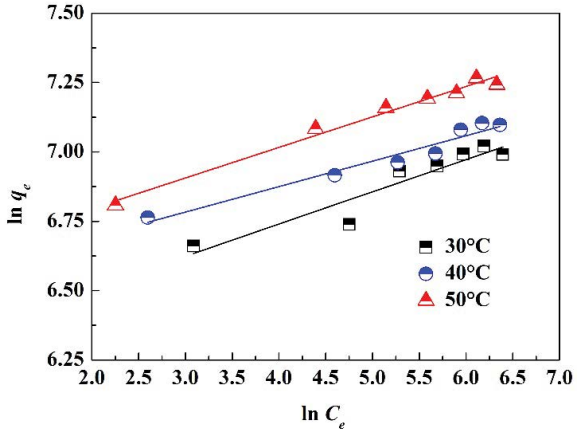

Fig. 12. Freundlich isotherms for adsorption of MB onto CnSACs.

Table 5
Dubinin–Radushkevich isotherm constants for the adsorption of MB

Adsorption temperature (°C)	30	40	50
q_m (mg/g)	1,033.804	1,126.758	1,331.418
B (mol²/J²)	2.247×10^{-5}	7.543×10^{-6}	5.342×10^{-6}
E (kJ/mol)	1.492	2.575	3.059
R^2	0.588	0.666	0.865

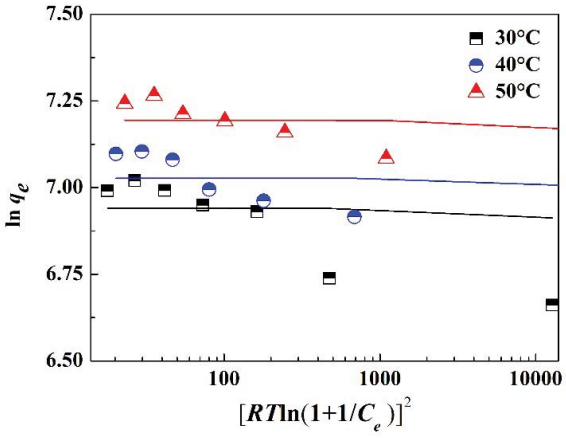

Fig. 13. Dubinin–Radushkevich isotherms for adsorption of MB onto a CnSACs.

adsorbate [46]. The values obtained for MB adsorption onto CnSACs were found to be 1.492, 2.575 and 3.059 kJ/mol at 304.15, 314.15 and 324.15 K, respectively. Therefore, the weak physical interactions are the driving force of MB onto CnSACs. However, the correlation coefficient (R^2) of the Dubinin–Radushkevich isotherm model is less than 0.7 when the temperature is 30°C and 40°C, thus the Dubinin–Radushkevich isotherm model does not fit the experimental data well.

3.4. Adsorption kinetic analysis

The adsorption kinetics of adsorbates onto activated carbons is complex, which can be influenced by the reactivity of adsorbent, the pH and temperature of the solutions, the surface and compositional features of adsorbate molecules, etc [47]. And the influence of these factors can be elucidated by investigating the experimental data using different kinetic models. In this work, four adsorption kinetic models, pseudo-first-order model, pseudo-second-order model, Elovich model and intraparticle diffusion model were used to analyze the adsorption kinetic experimental data.

The adsorption kinetic analysis of MB onto CnSACs was performed at temperatures of 30°C, 40°C and 50°C, respectively. The initial concentration of MB aqueous solution is 300 mg/L. As shown in Fig. 14, the adsorption capacity of MB increased with the increase of adsorption

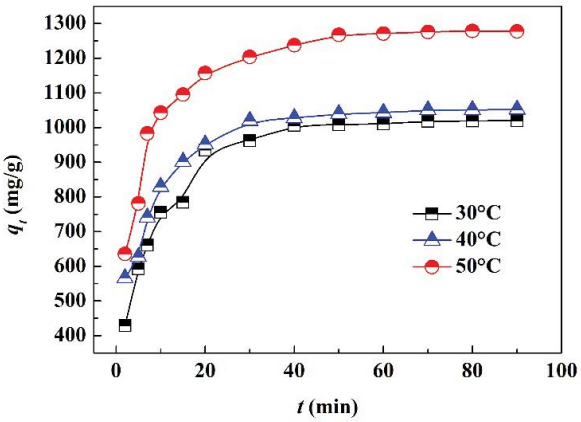

Fig. 14. Adsorption kinetics of MB molecules onto CnSACs at different solution temperatures.

time. Besides, the adsorption rate increased faster initial and grow slower after. This can be explained that sufficient adsorption active sites on the surface of CnSACs existed firstly. However, the active sites were occupied by MB gradually along with the increase of adsorption time.

3.4.1. Pseudo-first-order model

The pseudo-first-order model relies on that the rate of occupation of adsorption sites is proportional to the number of unoccupied sites [48], which is shown in Eq. (8):

$$\ln\left(q_{e,\mathrm{cal}} - q_t\right) = \ln q_{e,\mathrm{cal}} - K_1 t \tag{8}$$

As shown in Table 6 and Fig. 15, the experimental adsorption capacity of MB are 1,023.38; 1,055.680 and 1,285.71 mg/g at 30°C, 40°C and 50°C, respectively. The calculated values obtained from Eq. (8) are 1,020.243; 1,052.0787 and 1,278.401. The results show that the pseudo-first-order model has a good fitting effect in the first 50 min, but there is a big difference between the experimental values an d values when the adsorption time is over 50 min. The same conclusion was obtained by many authors [49–51].

3.4.2. Pseudo-second-order model

The pseudo-second-order kinetic model assumes that the adsorption rate is determined by the square of the number of unoccupied adsorption vacancies on the adsorbent surface, which is expressed as a linear form [52,53]:

$$\frac{t}{q_t} = \frac{1}{k_2 q_{e,\mathrm{cal}}^2} + \frac{1}{q_{e,\mathrm{cal}}} t \tag{9}$$

And as shown in Table 7 and Fig. 16, the pseudo-second-order model fitted the experimental data better than the pseudo-first-order model with a higher correlation coefficient (R^2) of more than 0.999. The results indicate that the adsorption capacity depends on the active sites

on the surface of CnSACs. Therefore, chemisorption may dominate the adsorption process [54].

3.4.3. Elovich model

Elovich model was firstly used in the kinetics of chemisorption of gases on solids, but now it has been successfully applied for the adsorption of solutes from a liquid solution. Elovich model is used to describe the chemical adsorption process, which is based on the assumption of surface energy inhomogeneity of adsorbed materials. The equation of the Elovich model is given as follows [55]:

$$q_t = \frac{1}{\beta}\ln\left(1+\alpha\beta t\right) \tag{10}$$

Table 6
Pseudo-first-order kinetics parameters for the adsorption of MB

Adsorption temperature (°C)	30	40	50
$q_{e,exp}$ (mg/g)	1,023.38	1,055.68	1,285.71
$q_{e,cal}$ (mg/g)	1,020.243	1,052.0787	1,278.401
K_1 (min^{-1})	0.0899	0.0913	0.0933
R^2	0.981	0.983	0.988

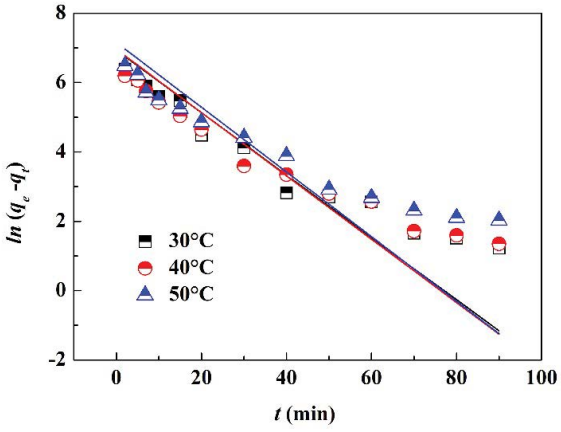

Fig. 15. Pseudo-first-order kinetics plots for the adsorption of MB onto CnSACs.

Table 7
Pseudo-second-order kinetics parameters for the adsorption of MB

Adsorption temperature (°C)	30	40	50
$q_{e,exp}$ (mg/g)	1,023.38	1,055.68	1,285.71
$q_{e,cal}$ (mg/g)	1,070.809	1,090.330	1,322.520
K_2 (min^{-1})	2.492×10^{-4}	3.241×10^{-4}	2.766×10^{-4}
R^2	0.9993	0.9997	0.9998

Fig. 17 shows the curve-fitting plots of the Elovich equation, and the kinetics parameters for the adsorption of MB are presented in Table 8. The linear relationship in Fig. 17 was obtained between the adsorption capacity of MB at different times, q_t, and $\ln(1 + \alpha\beta t)$, with correlation coefficients between 0.927 and 0.945. Compared with the correlation coefficients of the pseudo-second-order model, the correlation coefficients of the Elovich model is lower relatively. Therefore, the Elovich model is inappropriate to describe the adsorption process of MB onto CnSACs. This may be due to the fact that the Elovich equation is mainly used to describe adsorption on highly heterogeneous adsorbents.

3.4.4. Intraparticle diffusion model

When the diffusion of MB molecules inside the activated carbon is the rate-limiting step, the adsorption data can be presented by Eq. (11) [56]:

$$q_t = k_i t^{1/2} \tag{11}$$

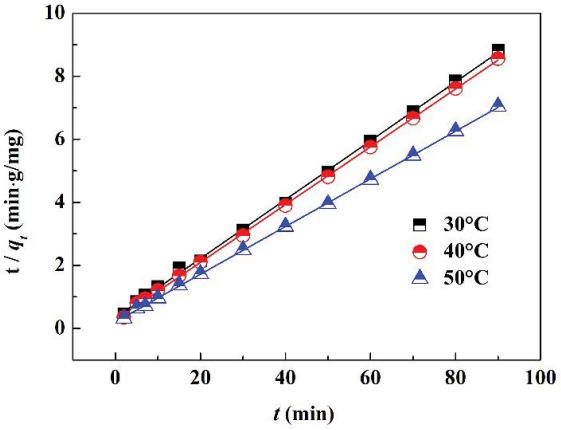

Fig. 16. Pseudo-second-order kinetics plots for the adsorption of MB onto CnSACs.

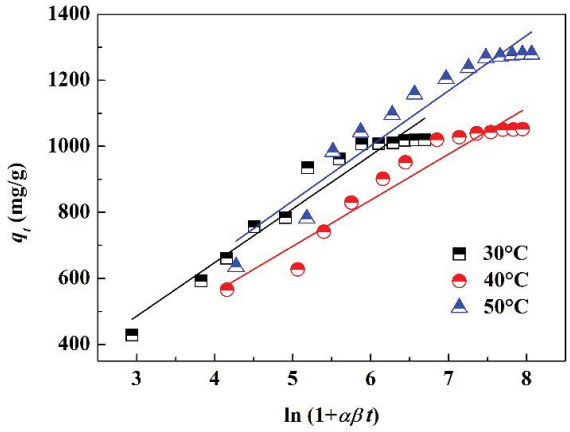

Fig. 17. Elovich kinetic plots for the adsorption of MB onto CnSACs.

where k_i is the intraparticle diffusion rate constant.

Fig. 18 presents the adsorption capacity of MB vs. $t^{1/2}$ at different temperature. The results showed that two or more steps occurred in the adsorption process. During the first stage, the adsorption rate was the fastest and the duration of this stage was about 20 min, and then the adsorption process entered the second stage, where intraparticle diffusion control was attained and continues from 20 to 50 min. Finally, the equilibrium adsorption started after 50 min. However, the correlation coefficients of this model are lower than 0.810 as shown in Table 9. The fittings results indicate that intraparticle diffusion is involved in the adsorption process and multiple limiting mechanisms exist. Moreover, surface adsorption and intraparticle diffusion may occur simultaneously, which control the adsorption kinetics of MB onto CnSACs.

Table 8
Elovich kinetics parameters for the adsorption of MB

Adsorption temperature (°C)	30	40	50
α	1,448.873	4,383.673	5,898.207
β	0.00617	0.00717	0.00599
R^2	0.945	0.936	0.927

3.5. Comparison of activated carbons prepared from raw materials

Based on the adsorption experimental data of MB onto CnSACs, the maximum adsorption value of MB is 1,489.88 mg/g under optimal conditions (impregnation mass ratio: 12.5, impregnation time: 27 h, activation temperature: 600°C, activation time: 75 min, initial MB dye concentration: 600 mg/L). Table 10 lists the comparison of adsorption capacity of MB onto activated carbons prepared from different materials. As shown in Table 10, the CnSACs have a bright application prospect in the treatment of colored wastewater.

4. Conclusion

In this work, a novel activated carbon prepared from the chestnut shell (CnSAC) has been used as an adsorbent

Table 9
Intraparticle diffusion kinetics parameters for the adsorption of MB

Adsorption temperature (°C)	30	40	50
k_i [mg/(g min$^{1/2}$)]	140.276	146.555	178.308
R^2	0.809	0.800	0.771

Table 10
Comparison of activated carbons prepared from different materials

Raw material	Activator	Maximum adsorption capacity, (mg/g)	Reference
Chestnut shell	$ZnCl_2$	1,489.88	This work
Rattan sawdust	KOH	294.12	Hameed et al. [22]
Jute fiber	Phosphoric acid	225.64	Senthilkumaar et al. [23]
Almond shell	$ZnCl_2$	1.33	Aygün et al. [24]
Walnut shell		3.53	
Hazelnut shell		8.82	
Apricot stone		4.11	
Rice hull	H_2SO_4	60.1	El-Halwany [25]
Cola nut shell	$ZnCl_2$	87.37	Ndi Nsami and Ketcha Mbadcam [26]
Dead leaves	$ZnCl_2$	149.85	Dural et al. [27]
Dross licorice	HCl and HNO_3	82.9	Ghaedi et al. [28]
Eucalyptus residue	H_3PO_4	977	Ahmed et al. [29]
Bamboo chip	KOH	305.3	Jawad and Abdulhameed [30]
Orange peel	KOH	382.15	Bediako et al. [31]
Mushroom	K_2CO_3	872	Sun et al. [32]
Liquefied wood	$ZnCl_2$	1,159	Ma et al. [33]
Date pits	$ZnCl_2$	455	Mahmoudi et al. [57]
Polyvinyl alcohol	$FeCl_3$	952.9	Jia et al. [58]
Used rubber slipper	KOH	60.2	Rajendaran et al. [59]
Asphaltenes	KOH	556	Han et al. [60]
Oil sludge	H_3PO_4	316.02	Li et al. [61]
Palm kernel shell	CaO	524.2	Ali et al. [62]
Oil palm empty fruit bunches	$ZnCl_2$	357	Sakamoto et al. [63]
Banana trunk waste	H_3PO_4	166.51	Danish et al. [64]

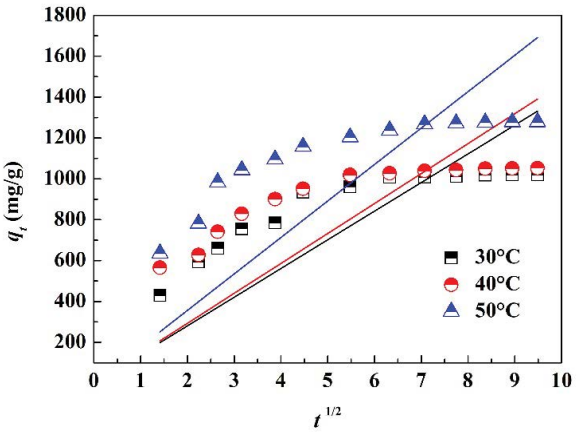

Fig. 18. Intraparticle diffusion kinetics plots for the adsorption of MB onto CnSACs.

for the removal of methylene blue (MB) dye from aqueous solutions. And 25 wt.% $ZnCl_2$ was used as the active agent. The results show that the adsorption capacity is influenced by preparation parameters (impregnation mass ratio, impregnation time, activation temperature, activation time), the dye solution pH and initial MB dye concentration. The maximum adsorption capacity of MB occurred at an initial pH of 5.0. And the maximum adsorption of MB onto the CnSACs is 1,489.88 mg/g. The CnSAC with the best adsorption capacity has a higher specific surface area reaching a value of 1,539.410 m^2/g. Moreover, equilibrium and kinetic studies were conducted for the adsorption of MB from aqueous solutions onto CnSACs. The adsorption isotherms of MB were fitted well by the Langmuir model, and the pseudo-second-order kinetic model provided the best correlation of the experimental data, which indicates that a chemisorption mechanism is a rate-controlling step. In addition, based on the comparison of adsorption of MB onto activated carbons prepared from different raw materials, it can be concluded that the CnSACs may be used as a low-cost, natural and abundant source for the treatment of the colored wastewater.

Acknowledgments

This work was supported by the Plan of Guidance and Cultivation for Young Innovative Talents of Shandong Province, the Doctoral Research Fund of Shandong Jianzhu University (X18068Z) and the Natural Science Foundation of Shandong Province (ZR2019BEE059, ZR2019BEE023, ZR2020QE204).

References

[1] Y.-S. Ho, T.-H. Chiang, Y.-M. Hsueh, Removal of basic dye from aqueous solution using tree fern as a biosorbent, Process Biochem., 40 (2005) 119–124.
[2] S. Mahbub, I. Shahriar, M. Iqfath, M.A. Hoque, M.A. Halim, M.A. Khan, M.A. Rub, A.M. Asiri, Influence of alcohols/electrolytes on the interaction of reactive red dye with surfactant and removal of dye from solutions, J. Environ. Chem. Eng., 7 (2019) 103364, doi: 10.1016/j.jece.2019.103364.
[3] A. Altaf, S. Noor, Q.M. Sharif, M. Najeebullah, Different techniques recently used for the treatment of textile dyeing effluents: a review, J. Chem. Soc. Pak., 32 (2010) 115–124.
[4] Y. Xiong, P.J. Strunk, H.Y. Xia, X.H. Zhu, H.T. Karlsson, Treatment of dye wastewater containing acid orange II using a cell with three-phase three-dimensional electrode, Water Res., 35 (2001) 4226–4230.
[5] W.S. Wan Ngah, C.S. Endud, R. Mayanar, Removal of copper(II) ions from aqueous solution onto chitosan and cross-linked chitosan beads, React. Funct. Polym., 50 (2002) 181–190.
[6] A. Aygun, B. Nas, M.F. Sevimli, Treatment of reactive dyebath wastewater by electrocoagulation process: optimization and cost-estimation, Korean J. Chem. Eng., 36 (2019) 1441–1449.
[7] P. Kasa, H. Papp, M. Pakaski, Presenilin-1 and its N-terminal and C-terminal fragments are transported in the sciatic nerve of rat, Brain Res., 909 (2001) 159–169.
[8] K.S. Lin, H.W. Cheng, W.R. Chen, C.F. Wu, Synthesis, characterization, and adsorption kinetics of titania nanotubes for basic dye wastewater treatment, Adsorption, 16 (2010) 47–56.
[9] W.S. Ou, G.Q. Zhang, X.J. Yuan, P. Su, Experimental study on coupling photocatalytic oxidation process and membrane separation for the reuse of dye wastewater, J. Water Process Eng., 6 (2015) 120–128.
[10] S. Raghu, C. Ahmed Basha, Chemical or electrochemical techniques, followed by ion exchange, for recycle of textile dye wastewater, J. Hazard. Mater., 149 (2007) 324–330.
[11] X.Y. Bi, P. Wang, C.Y. Jiao, H.L. Cao, Degradation of remazol golden yellow dye wastewater in microwave enhanced ClO_2 catalytic oxidation process, J. Hazard. Mater., 168 (2009) 895–900.
[12] A. Maezawa, H. Nakadoi, K. Suzuki, T. Furusawa, Y. Suzuki, S. Uchida, Treatment of dye wastewater by using photocatalytic oxidation with sonication, Ultrason. Sonochem., 14 (2007) 615–620.
[13] R. Rosal, A. Rodríguez, J.A. Perdigón-Melón, A. Petre, E. García-Calvo, M.J. Gómez, A. Agüera, A.R. Fernández-Alba, Occurrence of emerging pollutants in urban wastewater and their removal through biological treatment followed by ozonation, Water Res., 44 (2010) 578–588.
[14] N.K. Amin, Removal of direct blue-106 dye from aqueous solution using new activated carbons developed from pomegranate peel: adsorption equilibrium and kinetics, J. Hazard. Mater., 165 (2009) 52–62.
[15] C.L. Zhao, H.L. Zheng, Y.J. Sun, S.J. Zhang, J.J. Liang, Y.Z. Liu, Y.Y. An, Evaluation of a novel dextran-based flocculant on treatment of dye wastewater: effect of kaolin particles, Sci. Total Environ., 640–641 (2018) 243–254.
[16] D.N. Taha, I.S. Samaka, Natural Iraqi palygorskite clay as low cost adsorbent for the treatment of dye containing industrial wastewater, J. Oleo Sci., 61 (2012) 729–736.
[17] L. Kang, Y.J. Zhang, L.L. Wang, L. Zhang, K. Zhang, L.C. Liu, Alkali-activated steel slag-based mesoporous material as a new photocatalyst for degradation of dye from wastewater, Integr. Ferroelectr., 162 (2015) 8–17.
[18] E. Lorenc-Grabowska, G. Gryglewicz, Adsorption characteristics of Congo Red on coal-based mesoporous activated carbon, Dyes Pigm., 74 (2007) 34–40.
[19] Y. Shi, J.W. Chen, J. Chen, R.A. Macleod, M. Malac, Preparation and evaluation of hydrotreating catalysts based on activated carbon derived from oil sand petroleum coke, Appl. Catal., A, 441–442 (2012) 99–107.
[20] T.H. Liou, Development of mesoporous structure and high adsorption capacity of biomass-based activated carbon by phosphoric acid and zinc chloride activation, Chem. Eng. J., 158 (2010) 129–142.
[21] M.O. Abdullah, I.A.W. Tan, L.S. Lim, Automobile adsorption air-conditioning system using oil palm biomass-based activated carbon: a review, Renewable Sustainable Energy Rev., 15 (2011) 2061–2072.
[22] B.H. Hameed, A.L. Ahmad, K.N.A. Latiff, Adsorption of basic dye (methylene blue) onto activated carbon prepared from rattan sawdust, Dyes Pigm., 75 (2007) 143–149.

[23] S. Senthilkumaar, P.R. Varadarajan, K. Porkodi, C.V. Subbhuraam, Adsorption of methylene blue onto jute fiber carbon: kinetics and equilibrium studies, J. Colloid Interface Sci., 284 (2005) 78–82.
[24] A. Aygün, S. Yenisoy-Karakaş, I. Duman, Production of granular activated carbon from fruit stones and nutshells and evaluation of their physical, chemical and adsorption properties, Microporous Mesoporous Mater., 66 (2003) 189–195.
[25] M.M. El-Halwany, Study of adsorption isotherms and kinetic models for Methylene Blue adsorption on activated carbon developed from Egyptian rice hull (Part II), Desalination, 250 (2010) 208–213.
[26] J. Ndi Nsami, J. Ketcha Mbadcam, The adsorption efficiency of chemically prepared activated carbon from cola nut shells by $ZnCl_2$ on methylene blue, J. Chem.-NY, 2013 (2013) 469170 (1–7), doi: 10.1155/2013/469170.
[27] M.U. Dural, L. Cavas, S.K. Papageorgiou, F.K. Katsaros, Methylene blue adsorption on activated carbon prepared from *Posidonia oceanica* (L.) dead leaves: kinetics and equilibrium studies, Chem. Eng. J., 168 (2011) 77–85.
[28] M. Ghaedi, M.D. Ghazanfarkhani, S. Khodadoust, N. Sohrabi, M. Oftade, Acceleration of methylene blue adsorption onto activated carbon prepared from dross licorice by ultrasonic: equilibrium, kinetic and thermodynamic studies, J. Ind. Eng. Chem., 20 (2014) 2548–2560.
[29] D.N. Ahmed, L.A. Naji, A.A.H. Faisal, N.A. Ansari, M. Naushad, Waste foundry sand/MgFe-layered double hydroxides composite material for efficient removal of Congo red dye from aqueous solution, Sci. Rep., 10 (2020) 2042, doi: 10.1038/s41598-020-58866-y.
[30] A.H. Jawad. A.S. Abdulhameed, Statistical modeling of methylene blue dye adsorption by high surface area mesoporous activated carbon from bamboo chip using KOH-assisted thermal activation, Energy Environ., 5 (2020) 456–469.
[31] J.K. Bediako, S. Lin, A.K. Sarkar, Y.F. Zhao, Y.S. Yun, Evaluation of orange peel-derived activated carbons for treatment of dye-contaminated wastewater tailings, Environ. Sci. Pollut. Res., 27 (2020) 1053–1068.
[32] Z.W. Sun, C. Srinivasakannan, L.S. Liang, X.H. Duan, Preparation and characterization of shiitake mushroom-based activated carbon with high adsorption capacity, Arabian J. Sci. Eng., 44 (2019) 5443–5456.
[33] R. Ma, X.X. Qin, Z.G. Liu, Y.L. Fu, Adsorption property, kinetic and equilibrium studies of activated carbon fiber prepared from liquefied wood by $ZnCl_2$ activation, Materials, 12 (2019) 1377, doi: 10.3390/ma12091377.
[34] Z.Y. Yao, J.H. Qi, L.H. Wang, Equilibrium, kinetic and thermodynamic studies on the biosorption of Cu(II) onto chestnut shell, J. Hazard. Mater., 174 (2010) 137–143.
[35] X. Ke, P.J. Li, Q.X. Zhou, Y. Zhang, T.H. Sun, Removal of heavy metals from a contaminated soil using tartaric acid, J. Environ. Sci. (China), 18 (2006) 727–733.
[36] D. Özçimen, A. Ersoy-Meriçboyu, A study on the carbonization of grapeseed and chestnut shell, Fuel Process. Technol., 89 (2008) 1041–1046.
[37] H.H. Abdel Ghafar, G.A.M. Ali, O.A. Fouad, S.A. Makhlouf, Enhancement of adsorption efficiency of methylene blue on Co_3O_4/SiO_2 nanocomposite, Desal. Water Treat., 53 (2015) 2980–2989.
[38] W.N.R. Wan Isahak, N. Hamzah, N.A.M. Nordin, M.W. Mohamed Hisham, M.A. Yarmo, Dehydration studies of biomass resources for activated carbon production using BET and XRD techniques, Adv. Mater. Res., 620 (2012) 491–495.
[39] S. Senthilkumaar, P. Kalaamani, K. Porkodi, P.R. Varadarajan, C.V. Subburaam, Adsorption of dissolved reactive red dye from aqueous phase onto activated carbon prepared from agricultural waste, Bioresour. Technol., 97 (2006) 1618–1625.
[40] X.N. Li, Q.Y. Xu, G.M. Han, W.Q. Zhu, Z.H. Chen, X.B. He, X.J. Tian, Equilibrium and kinetic studies of copper(II) removal by three species of dead fungal biomasses, J. Hazard. Mater., 165 (2009) 469–474.
[41] S.M.S. Arabi, R.S. Lalehloo, M.R.T.B. Olyai, G.A.M. Ali, H. Sadegh, Removal of congo red azo dye from aqueous solution by ZnO nanoparticles loaded on multiwall carbon nanotubes, Physica E, 106 (2019) 150–155.
[42] H. Demiral, İ. Demiral, F. Tümsek, B. Karabacakoğlu, Adsorption of chromium(VI) from aqueous solution by activated carbon derived from olive bagasse and applicability of different adsorption models, Chem. Eng. J., 144 (2008) 188–196.
[43] P.S. Kumar, S. Ramalingam, S.D. Kirupha, A. Murugesan, T. Vidhyadevi, S. Sivanesan, Adsorption behavior of nickel(II) onto cashew nut shell: equilibrium, thermodynamics, kinetics, mechanism and process design, Chem. Eng. J., 167 (2011) 122–131.
[44] V.K. Gupta, S. Agarwal, H. Sadegh, G.A.M. Ali, A.K. Bharti, A.S.H. Makhlouf, Facile route synthesis of novel graphene oxide-β-cyclodextrin nanocomposite and its application as adsorbent for removal of toxic bisphenol A from the aqueous phase, J. Mol. Liq., 237 (2017) 466–472.
[45] S. Agarwal, H. Sadegh, M. Monajjemi, A.S. Hamdy, G.A.M. Ali, A.O.H. Memar, R. Shahryari-ghoshekandi, I. Tyagi, V.K. Gupta, Efficient removal of toxic bromothymol blue and methylene blue from wastewater by polyvinyl alcohol, J. Mol. Liq., 218 (2016) 191–197.
[46] R. Apiratikul, P. Pavasant, Batch and column studies of biosorption of heavy metals by *Caulerpa lentillifera*, Bioresour. Technol., 99 (2008) 2766–2777.
[47] A.L. Cazetta, O. Pezoti, K.C. Bedin, T.L. Silva, A. Paesano Jr., T. Asefa, V.C. Almeida, Magnetic activated carbon derived from biomass waste by concurrent synthesis: efficient adsorbent for toxic dyes, ACS Sustainable Chem. Eng., 4 (2016) 1058–1068.
[48] R. Rakhshaee, M. Khosravi, M.T. Ganji, Kinetic modeling and thermodynamic study to remove Pb(II), Cd(II), Ni(II) and Zn(II) from aqueous solution using dead and living *Azolla filiculoides*, J. Hazard. Mater., 134 (2006) 120–129.
[49] E. Bulut, M. Özacar, İ.A. Şengil, Adsorption of malachite green onto bentonite: equilibrium and kinetic studies and process design, Microporous Mesoporous Mater., 115 (2008) 234–246.
[50] B.H. Hameed, D.K. Mahmoud, A.L. Ahmad, Equilibrium modeling and kinetic studies on the adsorption of basic dye by a low-cost adsorbent: coconut (*Cocos nucifera*) bunch waste, J. Hazard. Mater., 158 (2008) 65–72.
[51] H.Y. Zhang, Y.A. Liu, X.W. Wu, X.Z. Jin, Z.J. Zhang, H. Zhao, J. Liu, Z.H. Huang, M.H. Fang, X. Min, Kinetics and equilibrium studies of the adsorption of methylene blue on *Euryale ferox* shell-based activated carbon, Micro Nano Lett., 13 (2018) 552–557.
[52] I.A.W. Tan, A.L. Ahmad, B.H. Hameed, Adsorption of basic dye on high-surface-area activated carbon prepared from coconut husk: equilibrium, kinetic and thermodynamic studies, J. Hazard. Mater., 154 (2008) 337–346.
[53] M. Naushad, Surfactant assisted nano-composite cation exchanger: development, characterization and applications for the removal of toxic Pb^{2+} from aqueous medium, Chem. Eng. J., 235 (2014) 100–108.
[54] S. Yusan, C. Gok, S. Erenturk, S. Aytas, Adsorptive removal of thorium(IV) using calcined and flux calcined diatomite from Turkey: evaluation of equilibrium, kinetic and thermodynamic data, Appl. Clay Sci., 67–68 (2012) 106–116.
[55] C. Gerente, V.K.C. Lee, P.L. Cloirec, G. McKay, Application of chitosan for the removal of metals from wastewaters by adsorption-mechanisms and models review, Crit. Rev. Env. Sci. Technol., 37 (2007) 41–127.
[56] H. Sadegh, G.A.M. Ali, Z. Abbasi, M.N. Nadagouda, Adsorption of ammonium ions onto multi-walled carbon nanotubes, Stud. Univ. Babes-Bolyai, Chem., 62 (2017) 233–245.
[57] K. Mahmoudi, K. Hosni, N. Hamdi, E. Srasra, Kinetics and equilibrium studies on removal of methylene blue and methyl orange by adsorption onto activated carbon prepared from date pits – a comparative study, Korean J. Chem. Eng., 32 (2014) 274–283.
[58] Z.G. Jia, Z.Y. Li, S.B. Li, Y.H. Li, R.S. Zhu, Adsorption performance and mechanism of methylene blue on chemically activated carbon spheres derived from hydrothermally-prepared poly(vinyl alcohol) microspheres, J. Mol. Liq., 220 (2016) 56–62.

[59] E. Rajendaran, M.A.A. Zaini, A. Arsad, N.S. Nasri, Carbon-based adsorbents from used rubber slipper for dye removal, Mater. Sci. Forum, 951 (2019) 83–88.
[60] Z.W. Han, S.L. Kong, J. Cheng, H. Sui, X.G. Li, Z.S. Zhang, L. He, Preparation of efficient carbon-based adsorption material using asphaltenes from asphalt rocks, Ind. Eng. Chem. Res., 58 (2019) 14785–14794.
[61] X.Y. Li, D. Han, M.Y. Zhang, B. Li, Z.B. Wang, Z.Q. Gong, P.K. Liu, Y.K. Zhang, X.H. Yang, Removal of toxic dyes from aqueous solution using new activated carbon materials developed from oil sludge waste, Colloids Surf., A, 578 (2019) 123505, doi: 10.1016/j.colsurfa.2019.05.066.
[62] G.A.M. Ali, O.A. Habeeb, H. Algarni, K.F. Chong, CaO impregnated highly porous honeycomb activated carbon from agriculture waste: symmetrical supercapacitor study, J. Mater. Sci., 54 (2018) 683–692.
[63] T. Sakamoto, M.A.Z. Abbas, Y. Amano, M. Machida, Preparation and characterization of activated carbons produced from oil palm empty fruit bunches, Tanso, 286 (2019) 9–13.
[64] M. Danish, T. Ahmad, S. Majeed, M. Ahmad, L. Ziyang, Z. Pin, I.S.M. Shakeel, Use of banana trunk waste as activated carbon in scavenging methylene blue dye: kinetic, thermodynamic, and isotherm studies, Bioresour. Technol. Rep., 3 (2018) 127–137.